Nonadiabatic nonlinear non-Hermitian quantized pumping

Motohiko Ezawa,[1] Natsuko Ishida,[2] Yasutomo Ota,[3] and Satoshi Iwamoto[2]
[1]*Department of Applied Physics, The University of Tokyo, 7-3-1 Hongo, Tokyo 113-8656, Japan*
[2]*Research Center for Advanced Science and Technology, The University of Tokyo, 4-6-1 Komaba, Tokyo 113-8656, Japan*
[3]*Research Center for Department of Applied Physics and Physico-Informatics, Keio University, 3-14-1 Hiyoshi, Japan*

(Received 3 November 2023; accepted 16 August 2024; published 6 September 2024)

We analyze a quantized pumping in a nonlinear non-Hermitian photonic system with nonadiabatic driving. The photonic system is made of a waveguide array, where the distances between adjacent waveguides are modulated. It is described by the Su-Schrieffer-Heeger model together with a saturated nonlinear gain term and a linear loss term. A topological interface state between the topological and the trivial phases is stabilized by the combination of a saturated nonlinear gain term and a linear loss term. We study the pumping of the topological interface state. We define the transfer-speed ratio ω/Ω by the ratio of the pumping speed ω of the center of mass of the wave packet to the driving speed Ω of the topological interface. It is quantized topologically as $\omega/\Omega = 1$ in the adiabatic limit. It remains to be quantized dynamically unless the driving is not too fast even in the nonadiabatic regime. On the other hand, the wave packet collapses and there is no quantized pumping when the driving is too fast. In addition, the stability against disorder is more enhanced by stronger nonlinearity.

DOI: 10.1103/PhysRevResearch.6.033258

I. INTRODUCTION

Topological insulator is a prominent idea in contemporary physics [1,2]. A typical example is a quantum Hall effect or a Chern insulator in a two-dimensional system described by the Chern number. The Thouless pump is a dynamical counterpart of a Chern insulator [3–6], where the Chern number is defined in the space-time variable. A pumped charge per one cycle is quantized. Especially, a topological-edge state is pumped in the quasicrystal model [7,8], the Rice-Mele model [9], and the Su-Schrieffer-Heeger (SSH) model [10].

Photonic systems provide us with an ideal playground of topological physics [11–21]. Various topological phases are realized in photonic crystal by modulating the hopping parameter spatially. A simplest example is the SSH model [22–26]. Especially, a large area topological interface laser is theoretically proposed by using the topological interface state of the SSH model [27,28]. The Thouless pumping is realized by using spatially modulated waveguides [7,8,29–31], where the hopping parameter between waveguides are spatially modulated by modulating the distances between the adjacent waveguides. Dynamics is governed by the Schrödinger equation [32,33], where the direction z of the waveguide acts as time t. Nonlinear Thouless pumping has been studied in photonic systems [34–38]. Recently, pumping by modulating the topological interface state of the SSH model is proposed in a linear Hermitian system [39], which is not the Thouless pumping.

Non-Hermiticity [40–42] and nonlinearity [43–47] naturally arises in topological photonics, which has expanded the field of topological physics starting from condensed matter physics. Photon loss is effectively well described by a non-Hermitian loss term. On the other hand, the gain has a saturation, which is described by a nonlinear term. Stable laser emission occurs in the presence of both of these terms [48,49]. The interplay of non-Hermiticity and nonlinearity is interesting [50–52]. It is understood in general that the Thouless pump is valid only in the adiabatic limit [53,54], although there exists a modification of the Thouless pump resulting in quantized nonadiabatic transport in the linear Hermitian case [55].

In this paper, we study a pumping in a nonlinear non-Hermitian photonic system. The basic structure is described by the SSH model, which has the topological and the trivial sectors. The topological interface state emerges around the interface between these two sectors. We investigate the pumping of this interface state by driving the interface. It is quantized topologically in the adiabatic limit. As long as the driving is not too fast, the motion of the interface state is synchronized with the motion of the interface and it remains to be quantized dynamically even in the nonadiabatic regime. This is because the interface state is stabilized dynamically by a nonlinear gain term and a linear loss term. On the other hand, when the driving is too fast, the synchronization is broken. The wave packet collapses and there is no quantized pumping. In addition, the stability against disorder is more enhanced by stronger nonlinearity.

II. MODEL AND INTERFACE STATE

We study a pumping of the topological interface state in the SSH model. The SSH model is the simplest model for topological insulators. It is a one-dimensional model with dimerized hopping parameters κ_A and κ_B as illustrated in Fig. 1. It has two phases, i.e., the trivial phase for $|\kappa_A| > |\kappa_B|$

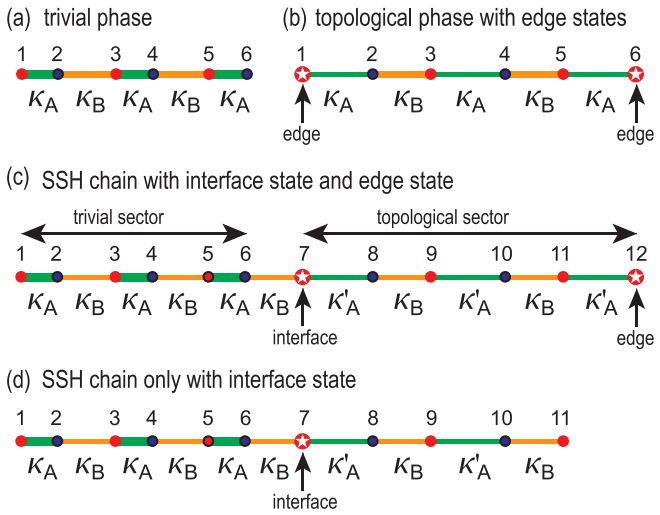

FIG. 1. SSH model is defined on a chain made of sites with dimerized hopping parameters κ_A and κ_B. The hopping parameter becomes larger when the distance between the adjacent sites is smaller. A green line indicates the hopping κ_A, while a yellow line indicates the hopping κ_B. The width of a line indicates the strength of the hopping. (a) It is in the trivial phase for $|\kappa_A| > |\kappa_B|$. (b) It is in the topological phase for $|\kappa_A| < |\kappa_B|$ together with the topological edge states at zero energy. (c) A single chain may contain both a trivial sector and a topological sector together with the interface state and the edge state at zero energy. Here, three hopping parameters $\kappa_A > \kappa_B > \kappa_A'$ are introduced. (d) The topological edge state can be removed from the spectrum by removing the edge site at $n = N + 1$ with $N = 11$. See Fig. 2 with respect to the energy and the profile of the topological interface state.

as in Fig. 1(a) and the topological phase for $|\kappa_A| < |\kappa_B|$ together with the topological edge states as in Fig. 1(b). We may consider the SSH model which contains both the trivial and the topological sectors, where one of the edge states turn into the interface state, as illustrated in Fig. 1(c). Furthermore, we remove the remaining edge state by removing the edge site as in Fig. 1(d). We focus on the interface state in the SSH chain of the type given by Fig. 1(d).

In the field of photonics, the SSH model is realized by an array of spatially modulated waveguides [7,8,14,29,31,56]. We consider N pillars on the (x, z) plane with z being the direction of the waveguide for $z \geqslant 0$. When an input is injected to the interface site $n_{\rm IF}$ at $z = 0$, the wave packet evolves mainly along the pillar. However, there are slight leaks along the x direction, which results in the hopping between adjacent pillars. When the spacing is large (small), the hopping is small (large).

A set of points on the pillars along the x axis at fixed z constitutes the SSH model [7,8,14,29,31,56], where the hopping parameter can be tuned by the spacing between the adjacent pillars and becomes a function of z. We tune the hopping parameters as follows:

$$\kappa_{A,n}(z) = \kappa\left(1 - \lambda \tanh\frac{n - n_{\rm IF}(z)}{\xi}\right), \quad \kappa_{B,n} = \kappa. \tag{1}$$

Note that $\kappa_{A,n}(z) > \kappa_B$ for $n < n_{\rm IF}(z)$, implying that the sector is trivial, while $\kappa_{A,n}(z) < \kappa_B$ for $n > n_{\rm IF}(z)$, implying that the sector is topological. Hence $n_{\rm IF}(z)$ is the position of the interface as a function of z. Here, $\lambda > 0$ and $\xi > 0$ represent the interface modulation amplitude and the interface width, respectively. Small (large) ξ represents a sharp (smooth) interface.

For definiteness, we choose the same site number N' for the trivial and the topological sectors, where N' is an even integer as illustrated in Figs. 1(a) and 1(b). Then, the interface position is given by $n_{\rm IF} = N' + 1$ as in Fig. 1(c). Next, we remove the right edge site in order to remove the topological edge state from the energy spectrum, as we have explained in Fig. 1(d). Hence the total site number is $N = 2N' - 1$. Then, the interface position is given by the site

$$n_{\rm IF} = \frac{N+1}{2} + 1. \tag{2}$$

Here, N is an odd integer such that $\frac{1}{2}(N + 1)$ is an even integer. In this work, we inject a pulse to the interface site $n_{\rm IF}$ at $z = 0$. The pulse evolves along the z direction. Then, we drive the interface $n_{\rm IF}(z)$ as a function of z. Its dynamics is governed by [48]

$$i\frac{d\psi_n}{dz} = \sum_m M_{nm}(z)\psi_m - i\gamma\left(1 - \chi\frac{[1-(-1)^n]/2}{1+|\psi_n|^2/\eta}\right)\psi_n, \tag{3}$$

where ψ_n is the amplitude at the site n with $n = 1, 2, 3, \ldots, N$. In this equation, M_{nm} is a z-dependent hopping matrix representing the SSH model,

$$M_{nm}(z) = \begin{pmatrix} 0 & \kappa_{A,n}(z) & 0 & 0 & 0 & \cdots \\ \kappa_{A,n}(z) & 0 & \kappa_B & 0 & 0 & \cdots \\ 0 & \kappa_B & 0 & \kappa_{A,n}(z) & 0 & \cdots \\ 0 & 0 & \kappa_{A,n}(z) & 0 & \kappa_B & \ddots \\ 0 & 0 & 0 & \kappa_B & 0 & \ddots \\ \vdots & \vdots & \vdots & \ddots & \ddots & \ddots \end{pmatrix}, \tag{4}$$

γ represents the constant loss in each waveguide, $\gamma\chi$ represents the amplitude of the optical gain via stimulated emission induced only at the odd site, and η represents the saturation parameter of nonlinear gain [48]. All these parameters are positive. The system turns out to be a linear non-Hermitian model in the limit $1/\eta \to 0$. On the other hand, γ controls simultaneously the nonlinearity and the non-Hermiticity as far as $1/\eta \neq 0$. The system is linear and Hermitian for $\gamma = 0$. In Eq. (3) we measure z in units of $1/\kappa$ and the loss parameter γ in units of κ, where κ is defined in Eq. (1).

An interface state emerging at the interface between the topological and the trivial sectors is obtained by solving the eigenequation $M_{nm}\psi_n = E\psi_n$ with the matrix M_{nm} given by Eqs. (1) and (4). We show the result in Fig. 2. There is one zero-energy state as in Fig. 2(a) representing the topological interface state, which is shown in Fig. 2(b). Note that we have removed the topological edge state by removing the corresponding edge site as illustrated in Fig. 1(d).

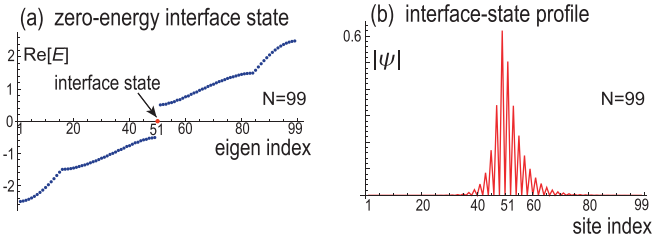

FIG. 2. (a) Energy spectrum of the SSH model (4) in the presence of the interface (1). There is only one zero-energy state representing the topological interface state. (b) The eigenfunction of the topological interface state. We have used a chain with $N = 99$. Then, the interface state emerges around $n_{\rm IF} = 51$ according to Eq. (2). We have set $\xi = 1$ and $\lambda = 0.5$.

The explicit equations for a finite chain with length N follow from Eq. (3) as

$$i\frac{d\psi_{2n-1}}{dz} = \kappa_B\psi_{2n-2} + \kappa_{A,n}(z)\psi_{2n} - i\gamma\left(1 - \frac{\chi}{1+|\psi_{2n-1}|^2/\eta}\right)\psi_{2n-1}, \quad (5)$$

$$i\frac{d\psi_{2n}}{dz} = \kappa_B\psi_{2n+1} + \kappa_{A,n}(z)\psi_{2n-1} - i\gamma\psi_{2n}. \quad (6)$$

We analyze them in the following.

III. RELAXATION PROCESS

We solve the set of Eqs. (5) and (6) by imposing the boundary condition

$$\psi_n(z=0) = \delta_{n,n_{\rm IF}}. \quad (7)$$

It is convenient to regard z as time t. Then, Eqs. (5) and (6) are the Schrödinger equations describing a quench dynamics starting from the interface site by giving an input to it with the initial condition (7). We consider the case where the interface position is given by Eq. (2) or

$$n_{\rm IF}(z) = \tfrac{1}{2}(N+1) + 1 \quad (8)$$

for the relaxation process $z < z_0$ and by

$$n_{\rm IF}(z) = \left[\tfrac{1}{2}(N+1) + 1\right] + \Omega(z - z_0) \quad (9)$$

for the driving process $z > z_0$. In what follows, we may occasionally regard z as time t. The pumping is said to be adiabatic for $\Omega \ll \kappa$, which means that any finite driving is nonadiabatic.

The relaxation process is necessary before the driving process, where the wave packet spreads from the delta function (7) and reaches the stational distribution as in Figs. 3(a1) and 3(b1). The interface state is formed in the relaxation process ($z < z_0$) to balance the nonlinear gain terms and the linear loss terms.

IV. ADIABATIC PUMPING

We investigate the driving process, where the interface position $n_{\rm IF}(z)$ is modulated as in Eq. (9) for $z > z_0$. We first consider the adiabatic driving, where the eigenfunction is well approximated by the snapshot solution using the adiabatic approximation. The eigenstate ψ_n is obtained by a stationary solution at each z by solving the equation

$$\sum_m M_{nm}(z)\psi_m - i\gamma\left(1 - \chi\frac{[1-(-1)^n]/2}{1+|\psi_n|^2/\eta}\right)\psi_n = 0. \quad (10)$$

The stationary solution is given by

$$\psi_n(z) = \psi_{n-n_{\rm IF}(z)}(z_0), \quad (11)$$

where the wave packet perfectly follows the interface without any deformation. It is numerically confirmed as in Fig. 3(a2).

V. TOPOLOGICAL PUMPING

We proceed to argue that the pumping is topological and it is quantized in the adiabatic limit. Although we have so far investigated a pumping phenomenon in an open SSH chain

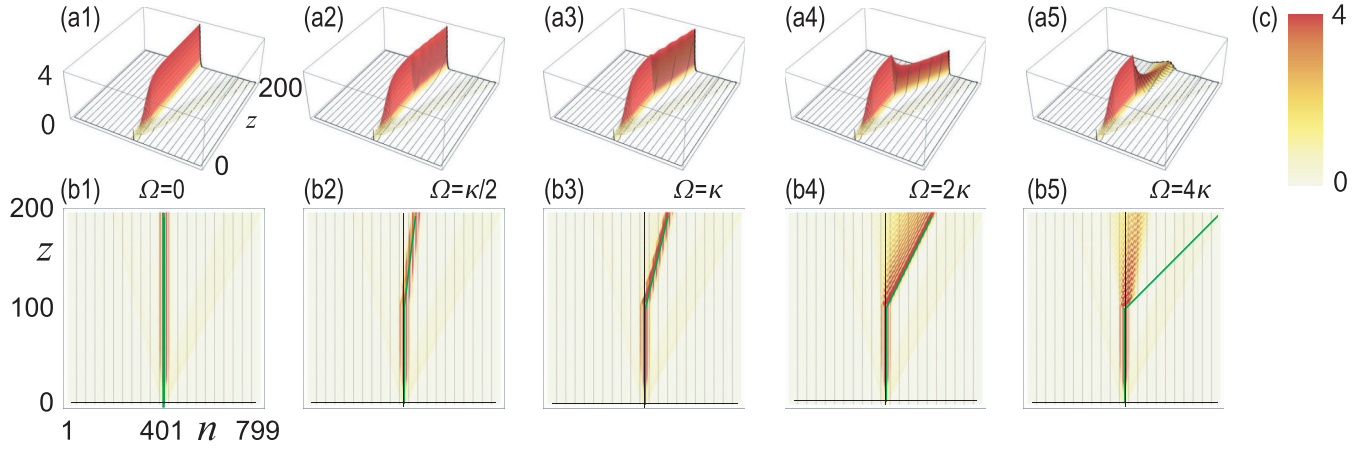

FIG. 3. Wave packet in quench dynamics in bird's eye view and in the (n, z) plane. (a1), (b1) $\Omega = 0$; (a2), (b2) $\Omega = \kappa/2$; (a3), (b3) $\Omega = \kappa$; (a4), (b4) $\Omega = 2\kappa$; (a5), (b5) $\Omega = 4\kappa$. We have used a chain with $N = 799$. We have set $\eta = 10$, $\xi = 20$, $\lambda = 0.5$, $\gamma = 0.1$, and $\chi = 1$. The evolution is calculated in the range $0 \leqslant z \leqslant 200$, where $z_0 = 100$. A green line represents the interface position $n_{\rm IF}(z)$ given by Eqs. (8) and (9). Here, $n_{\rm IF}(z) = 401$ in the relaxation process ($z \leqslant 100$). (c) The color palette showing the absolute value of the wave function.

with length N, we may consider torus geometry by identifying $n = N$ as $n = 1$. Then, because the driving is periodic, $\Omega(z_0 + N/\Omega) = \Omega(z_0)$, we identify $z = z_0$ and $z = z_0 + N/\Omega$. In the periodic system, according to the definition of polarization by King-Smith and Vanderbilt [57], the mean position (16) is rewritten as

$$\langle x(z)\rangle = \int \langle \psi_{k_x}(z)| \frac{\partial}{i\partial k_x} |\psi_{k_x}(z)\rangle dk_x, \tag{12}$$

where $\psi_{k_x}(z)$ is the Fourier transform of $\psi_n(z)$, for which we may use the wave function of the interface state as far as the motion of the interface state and the motion of the interface are synchronized. The formula (12) implies that $\langle x(z)\rangle$ is a phase of the wave function $\psi_{k_x}(z)$ and hence it can be multivalued.

Then, the topological number P is the winding number,

$$P = \frac{1}{N}\int_{z_0}^{z_0+N/\Omega} \frac{\partial \langle x(z)\rangle}{\partial z} dz, \tag{13}$$

which is the pumped charge when the interface shifts by N sites. We now insert Eq. (13) to Eq. (17) to obtain $P = \omega/\Omega$.

In the adiabatic limit, the mean position is exactly given by

$$\langle x(z)\rangle = n_{\rm IF}(z) = \Omega(z - z_0) \tag{14}$$

by using Eq. (11). By inserting it to the winding number (13), we obtain the winding number is quantized to be 1.

VI. NONADIABATIC PUMPING

Next, we study nonadiabatic driving numerically. What is unexpected is the numerical result for larger values of Ω. For slow driving $\Omega < \kappa$, the wave packet is stabilized as in Figs. 3(a1)–3(a3), whose motion is perfectly synchronized with the motion of the interface described by Eq. (9), as shown by the green line in Figs. 3(b1)–3(b3). On the other hand, for fast driving $\Omega > \kappa$, the wave packet collapses and spreads, as shown in Figs. 3(b4)–3(a5) and 3(b4)–3(b5).

To investigate these phenomena quantitatively, we calculate the fidelity defined by

$$F(z) \equiv |\langle \psi_{n-n_{\rm IF}(z)}(0)|\psi_n(z)\rangle|. \tag{15}$$

The wave packet synchronizes perfectly with the moving interface in the adiabatic limit and is well described by $|\psi_n(z)| = |\psi_{n-n_{\rm IF}(z)}(0)|$, or $F(z) = 1$ as $\Omega/\kappa \to 0$. We show the fidelity at $z = 200$ in Fig. 4(a) as a function of the driving speed Ω for various values of the parameter γ. The fidelity is almost 1 in a wide range of Ω/κ unless $\gamma = 0$ and this range becomes wider as γ increases, where the wave packet is pumped without changing its form. It fluctuates around 1 in the linear Hermitian model ($\gamma = 0$). On the other hand, the fidelity decreases rapidly as a further increase of Ω. It means that the driving is too fast for the wave packet to follow it.

To determine the pumping velocity, we calculate the expectation value of the mean position by

$$\langle x(z)\rangle \equiv \frac{\sum_n [n - n_{\rm IF}(0)]|\psi_n(z)|^2}{\sum_n |\psi_n(z)|^2}. \tag{16}$$

We show the z evolution of $\langle x(z)\rangle$ for various Ω in Fig. 5(a). It is almost zero in the relaxation process ($z < z_0$). On the other hand, it increases almost linearly in the driving process

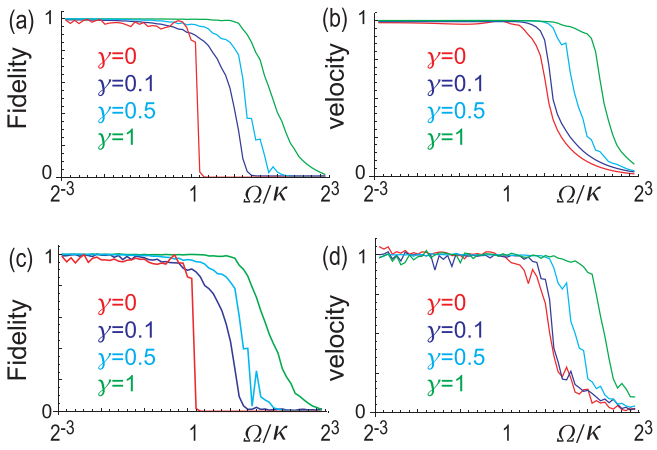

FIG. 4. (a) Fidelity as a function of Ω/κ for various γ. (b) Ratio ω/Ω as a function of Ω/κ for various γ. The horizontal axis is in the logarithmic scale ($\log_2 \Omega/\kappa$). (c) Fidelity in the presence of disorder $\zeta = 0.1$. (d) Ratio in the presence of disorder $\zeta = 0.1$. Calculations are done for a specific configuration of randomness. Red curves indicate $\gamma = 0$ (the linear model), blue curves indicate $\gamma = 0.1$, green curves indicate $\gamma = 1$, and cyan curves indicate $\gamma = 4$.

($z > z_0$). Namely, $\langle x(z)\rangle$ is well approximated by

$$\langle x(z)\rangle = \omega(z - z_0). \tag{17}$$

We define the pumping velocity ω at each Ω by this formula.

We then calculate numerically the transfer-speed ratio ω/Ω. We plot the ratio ω/Ω as a function of Ω/κ for various γ in Fig. 4(c), where it is found that the pumping speed is almost identical to the driving speed, i.e., $\omega = \Omega$, in a wide range of Ω/κ, and this range becomes wider as γ increases as in the case of the fidelity.

These phenomena are interpreted as follows. The wave packet is dynamically stabilized by the nonlinear gain term and the linear loss term. These terms act as a restoring force for a wave packet for slow driving.

We have estimated $\log_{10}|1 - \omega/\Omega|$ in order to see how ω/Ω is quantized. It is found to be of the order of 10^{-6} for $\Omega/\kappa = 2^{-10}$: see Fig. 5(b). Namely, the ratio ω/Ω is of the order of 0.999999 for $\Omega/\kappa = 2^{-10}$. In addition, the accuracy is more enhanced for slower driving.

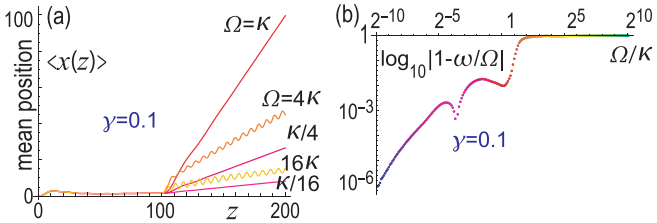

FIG. 5. (a) Evolution of the mean position $\langle x(z)\rangle$. The pumping velocity ω is determined from the slope of the line for each Ω/κ. The horizontal axis is z with $0 \leqslant z \leqslant 200$. (b) $\log_{10}|\omega/\Omega - 1|$ as a function of Ω. We have set $\eta = 10$, $\xi = 20$, $\lambda = 0.5$, $\gamma = 0.1$, and $\chi = 1$.

VII. SCALE INVARIANCE

We discuss the effect of the nonlinear saturation η. By making a scale transformation

$$\psi_{2n-1} \mapsto \sqrt{\eta}\psi'_{2n-1}, \tag{18}$$

Eq. (3) is rewritten as

$$i\frac{d\psi'_n}{dz} = \sum_{nm} M_{nm}\psi'_m - i\gamma\left(1 - \chi\frac{[1-(-1)^n]/2}{1+|\psi'_n|^2}\right)\psi'_n, \tag{19}$$

with the initial condition $\psi_n(z=0) = \sqrt{\eta}\delta_{n,n_{\rm IF}}$, where the nonlinear saturation is found to be normalized. Because the saturated wave packet is independent of the initial condition, there is a scale invariance in the fidelity and the transfer-speed ratio as a function of η as far as $1/\eta \neq 0$. Namely, they are irrelevant to the magnitude of η. On the other hand, the wave packet diverges due to the gain term in the linear non-Hermitian model ($\gamma \neq 0$, $1/\eta = 0$).

VIII. DISORDER EFFECT

We study disorder effects. We introduce uniformly distributing randomness from $-\zeta_n(z)$ to $\zeta_n(z)$ to the hopping parameters at each z and site n as

$$\kappa_{A,n}(z) = \kappa\left(1 + \lambda\,\tanh\frac{n - n_{\rm IF}(z)}{\xi} + \zeta_n(z)\right), \tag{20}$$

$$\kappa_{B,n}(z) = \kappa[1 + \zeta_n(z)]. \tag{21}$$

The fidelity and the mean velocity are calculated with the 10% randomness for specific configuration of randomness, whose results are shown in Fig. 4. The fidelity is found to be robust in the presence of disorder. Especially, stability is more enhanced by stronger nonlinearity as shown in Fig. 4(c). Similarly, the velocity is also found to be robust in the presence of disorder. Especially, the stability is more enhanced for stronger nonlinearity as shown in Fig. 4(d). In conclusion, the pumping is robust against disorder even in the nonadiabatic regime, where the stability is enhanced by strong nonlinearity.

IX. DISCUSSIONS

The nonlinear non-Hermitian pumping is quantized topologically in the adiabatic limit. We have shown that the nonlinear non-Hermitian pumping is quantized dynamically even in the nonadiabatic regime. The combination of the saturated gain and the linear loss stabilizes the wave packet dynamically and hence it is robust even for nonadiabatic driving as long as the driving speed is not too fast. Our work provides an example that the interplay among non-Hermiticity and nonlinearity gives an intriguing phenomena in the nonadiabatic regime.

Femto-second laser writing waveguide [14,58,59] or semiconductor waveguide [60–62] are used in experiments. Typical distance between waveguides is 15 μm (5 μm) and the length of the waveguide is 500 mm (50 μm) for a femtosecond laser writing [14] (semiconductor [62]) waveguide. We have set $N = 799$, which corresponds to 12 mm for a femtosecond laser writing waveguide and 4 mm for a semiconductor waveguide, in numerical simulations.

Loss is introduced by using a lossy photonic crystal [63] and waveguides [64,65]. Gain is provided through two-wave mixing using the material's photorefractive nonlinearity [66–68] or optical pumping [69–72].

ACKNOWLEDGMENTS

M.E. is supported by CREST, JST (Grant No. JPMJCR20T2) and Grants-in-Aid for Scientific Research from MEXT KAKENHI (Grant No. 23H00171). N.I. is supported by the Grants-in-Aid for Scientific Research from MEXT KAKENHI (Grant No. JP21J40088). Y.O. is supported by the Grants-in-Aid for Scientific Research from MEXT KAKENHI (Grants No. 22H01994 and No. 22H00298). S.I. is supported by CREST, JST (Grant No. JPMJCR19T1) and the Grants-in-Aid for Scientific Research from MEXT KAKENHI (Grants No. 22H00298 and No. 22H01994).

[1] M. Z. Hasan and C. L. Kane, *Colloquium:* Topological insulators, Rev. Mod. Phys. **82**, 3045 (2010).
[2] X.-L. Qi and S.-C. Zhang, Topological insulators and superconductors, Rev. Mod. Phys. **83**, 1057 (2011).
[3] D. J. Thouless, Quantization of particle transport, Phys. Rev. B **27**, 6083 (1983).
[4] Q. Niu and D. J. Thouless, Quantised adiabatic charge transport in the presence of substrate disorder and many-body interaction, J. Phys. A: Math. Gen. **17**, 2453 (1984).
[5] Q. Niu, Towards a quantum pump of electric charges, Phys. Rev. Lett. **64**, 1812 (1990).
[6] R. Citro and M. Aidelsburger, Thouless pumping and topology, Nat. Rev. Phys. **5**, 87 (2023).
[7] Y. E. Kraus, Y. Lahini, Z. Ringel, M. Verbin, and O. Zilberberg, Topological states and adiabatic pumping in quasicrystals, Phys. Rev. Lett. **109**, 106402 (2012).
[8] M. Verbin, O. Zilberberg, Y. Lahini, Y. E. Kraus and Y. Silberberg, Topological pumping over a photonic Fibonacci quasicrystal, Phys. Rev. B **91**, 064201 (2015).
[9] R. Wang, X. Z. Zhang, and Z. Song, Dynamical topological invariant for the non-Hermitian Rice-Mele model, Phys. Rev. A **98**, 042120 (2018).
[10] S. Longhi, Topological pumping of edge states via adiabatic passage, Phys. Rev. B **99**, 155150 (2019).
[11] F. D. M. Haldane and S. Raghu, Possible realization of directional optical waveguides in photonic crystals with broken time-reversal symmetry, Phys. Rev. Lett. **100**, 013904 (2008).
[12] A. B. Khanikaev, S. H. Mousavi, W.-K. Tse, M. Kargarian, A. H. MacDonald, and G. Shvets, Photonic topological insulators, Nat. Mater. **12**, 233 (2013).

[13] M. Hafezi, E. Demler, M. Lukin, and J. Taylor, Robust optical delay lines with topological protection, Nat. Phys. **7**, 907 (2011).

[14] M. C. Rechtsman, J. M. Zeuner, Y. Plotnik, Y. Lumer, D. Podolsky, F. Dreisow, S. Nolte, M. Segev, and A. Szameit, Photonic Floquet topological insulators, Nature (London) **496**, 196 (2013).

[15] M. Hafezi, S. Mittal, J. Fan, A. Migdall, and J. Taylor, Imaging topological edge states in silicon photonics, Nat. Photon. **7**, 1001 (2013).

[16] L. H. Wu and X. Hu, Scheme for achieving a topological photonic crystal by using dielectric material, Phys. Rev. Lett. **114**, 223901 (2015).

[17] A. B. Khanikaev and G. Shvets, Two-dimensional topological photonics, Nat. Photon. **11**, 763 (2017).

[18] L. Lu. J. D. Joannopoulos, and M. Soljacic, Topological photonics, Nat. Photon. **8**, 821 (2014).

[19] T. Ozawa, H. M. Price, A. Amo, N. Goldman, M. Hafezi, L. Lu, M. C. Rechtsman, D. Schuster, J. Simon, O. Zilberberg, and L. Carusotto, Topological photonics, Rev. Mod. Phys. **91**, 015006 (2019).

[20] Y. Ota, K. Takata, T. Ozawa, A. Amo, Z. Jia, B. Kante, M. Notomi, Y. Arakawa, and S. Iwamoto, Active topological photonics, Nanophotonics **9**, 547 (2020).

[21] S. Iwamoto, Y. Ota, and Y. Arakawa, Recent progress in topological waveguides and nanocavities in a semiconductor photonic crystal platform, Opt. Mater. Express **11**, 319 (2021).

[22] P. St-Jean, V. Goblot, E. Galopin, A. Lemaitre, T. Ozawa, L. Le Gratiet, I. Sagnes, J. Bloch, and A. Amo, Lasing in topological edge states of a one-dimensional lattice, Nat. Photon. **11**, 651 (2017).

[23] M. Parto, S. Wittek, H. Hodaei, G. Harari, M. A. Bandres, J. Ren, M. C. Rechtsman, M. Segev, D. N. Christodoulides, and M. Khajavikhan, Edge-mode lasing in 1D topological active arrays, Phys. Rev. Lett. **120**, 113901 (2018).

[24] H. Zhao, P. Miao, M. H. Teimourpour, S. Malzard, R. El-Ganainy, H. Schomerus, and L. Feng, Topological hybrid silicon microlasers, Nat. Commun. **9**, 981 (2018).

[25] C. Han, M. Lee, S. Callard, C. Seassal, and H. Jeon, Lasing at topological edge states in a photonic crystal L3 nanocavity dimer array, Light: Sci. Appl. **8**, 40 (2019).

[26] Y. Ota, R. Katsumi, K. Watanabe, S. Iwamoto, and Y. Arakawa, Topological photonic crystal nanocavity laser, Commun. Phys. **1**, 86 (2018).

[27] N. Ishida, Y. Ota, W. Lin, T. Byrnes, Y. Arakawa, and S. Iwamoto, A large-scale single-mode array laser based on a topological edge mode, Nanophotonics **11**, 2169 (2022).

[28] M. Ezawa, N. Ishida, Y. Ota, and S. Iwamoto, Supersymmetric non-Hermitian topological interface laser, Phys. Rev. B **107**, 085302 (2023).

[29] Y. E. Kraus, Z. Ringel, and O. Zilberberg, Four-dimensional quantum Hall effect in a two-dimensional quasicrystal, Phys. Rev. Lett. **111**, 226401 (2013).

[30] Y. Ke, X. Qin, F. Mei, H. Zhong, Y. S. Kivshar, and C. Lee, Topological phase transitions and Thouless pumping of light in photonic waveguide arrays, Laser Photon. Rev. **10**, 995 (2016).

[31] O. Zilberberg, S. Huang, J. Guglielmon, M. Wang, K. P. Chen, Y. E. Kraus, and M. C. Rechtsman, Photonic topological boundary pumping as a probe of 4D quantum Hall physics, Nature (London) **553**, 59 (2018).

[32] S. G. Krivoshlykov, *Quantum-Theoretical Formalism for Inhomogeneous Graded-Index Waveguides* (Akademie Verlag, Berlin, 1994).

[33] S. Longhi, Quantum-optical analogies using photonic structures, Laser Photon. Rev. **3**, 243 (2009).

[34] M. Jürgensen and M. C. Rechtsman, Chern number governs soliton motion in nonlinear Thouless pumps, Phys. Rev. Lett. **128**, 113901 (2022).

[35] M. Jurgensen, S. Mukherjee, C. Jörg, and M. C. Rechtsman, Fractionally quantized topological nonlinear Thouless pumping of solitons, Nat. Phys. **19**, 420 (2023).

[36] N. Mostaan, F. Grusdt, and N. Goldman, Quantized topological pumping of solitons in nonlinear photonics and ultracold atomic mixtures, Nat. Commun. **13**, 5997 (2022).

[37] Q. Fu, P. Wang, Y. V. Kartashov, V. V. Konotop, and F. Ye, Nonlinear Thouless pumping: solitons and transport breakdown, Phys. Rev. Lett. **128**, 154101 (2022).

[38] Q. Fu, P. Wang, Y. V. Kartashov, V. V. Konotop, and F. Ye, Two-dimensional nonlinear Thouless pumping of matter waves, Phys. Rev. Lett. **129**, 183901 (2022).

[39] J. Yuan. C. Xu, H. Cai, and D.-W. Wang, Gap-protected transfer of topological defect states in photonic lattices, APL Photon. **6**, 030803 (2021).

[40] L. Feng, R. El-Ganainy, and L. Ge, Non-Hermitian photonics based on parity–time symmetry, Nat. Photon. **11**, 752 (2017).

[41] S. Weimann, M. Kremer, Y. Plotnik, Y. Lumer, S. Nolte, K. G. Makris, M. Segev, M. C. Rechtsman, and A. Szameit, Topologically protected bound states in photonic parity–time-symmetric crystals, Nat. Mater. **16**, 433 (2017).

[42] R. El-Ganainy, K. G. Makris, M. Khajavikhan, Z. H. Musslimani, S. Rotter, and D. N. Christodoulides, Non-Hermitian physics and PT symmetry, Nat. Phys. **14**, 11 (2018).

[43] D. Leykam and Y. D. Chong, Edge solitons in nonlinear-photonic topological insulators, Phys. Rev. Lett. **117**, 143901 (2016).

[44] X. Zhou, Y. Wang, D. Leykam, and Y. D. Chong, Optical isolation with nonlinear topological photonics, New J. Phys. **19**, 095002 (2017).

[45] S. Malzard and H. Schomerus, Nonlinear mode competition and symmetry-protected power oscillations in topological lasers, New. J. Phys. **20**, 063044 (2018).

[46] D. Smirnova, D. Leykam, Y. Chong, and Y. Kivshar, Nonlinear topological photonics, Appl. Phys. Rev. **7**, 021306 (2020).

[47] M. Ezawa, Nonlinearity-induced transition in the nonlinear Su-Schrieffer-Heeger model and a nonlinear higher-order topological system, Phys. Rev. B **104**, 235420 (2021).

[48] G. Harari, M. A. Bandres, Y. Lumer, M. C. Rechtsman, Y. D. Chong, M. Khajavikhan, D. N. Christodoulides, and M. Segev, Topological insulator laser: Theory, Science **359**, eaar4003 (2018).

[49] M. A. Bandres, S. Wittek, G. Harari, M. Parto, J. Ren, M. Segev, D. N. Christodoulides, and M. Khajavikhan, Topological insulator laser: Experiments, Science **359**, eaar4005 (2018).

[50] A. U. Hassan, H. Hodaei, M. A. Miri, M. Khajavikhan, and D. N. Christodoulides, Nonlinear reversal of the *PT*-symmetric phase transition in a system of coupled semiconductor microring resonators, Phys. Rev. A **92**, 063807 (2015).

[51] S. Malzard, E. Cancellieri, and H. Schomerus, Topological dynamics and excitations in lasers and condensates with saturable gain or loss, Opt. Express **26**, 22506 (2018).

[52] M. Ezawa, Nonlinear non-Hermitian higher-order topological laser, Phys. Rev. Res. **4**, 013195 (2022).

[53] L. Privitera, A. Russomanno, R. Citro, and G. E. Santoro, Nonadiabatic breaking of topological pumping, Phys. Rev. Lett. **120**, 106601 (2018).

[54] T. Tuloup, R. W. Bomantara, and J. Gong, Breakdown of quantization in nonlinear Thouless pumping, New J. Phys. **25**, 083048 (2023).

[55] S. Malikis and V. Cheianov, An ideal rapid-cycle Thouless pump, SciPost Phys. **12**, 203 (2022).

[56] I. L. Garanovich, S. Longhi, A. A. Sukhorukov, and Y. S. Kivshar, Light propagation and localization in modulated photonic lattices and waveguides, Phys. Rep. **518**, 1 (2012).

[57] R. D. King-Smith and D. Vanderbilt, Theory of polarization of crystalline solids, Phys. Rev. B **47**, 1651(R) (1993); First-principles investigation of ferroelectricity in perovskite compounds, **49**, 5828 (1994).

[58] K. M. Davis, K. Miura, N. Sugimoto, and K. Hirao, Writing waveguides in glass with a femtosecond laser, Opt. Lett. **21**, 1729 (1996).

[59] A. Szameit and S. Nolte, Discrete optics in femtosecond-laser-written photonic structures, J. Phys. B: At. Mol. Opt. Phys. **43**, 163001 (2010).

[60] J. S. Foresi, P. R. Villeneuve, J. Ferrera, E. R. Thoen, G. Steinmeyer, S. Fan, J. D. Joannopoulos, L. C. Kimerling, H. I. Smith, and E. P. Ippen, Photonic-bandgap microcavities in optical waveguides, Nature (London) **390**, 143 (1997).

[61] M. A. Foster, A. C. Turner, J. E. Sharping, B. S. Schmidt, M. Lipson, and A. L. Gaeta, Broad-band optical parametric gain on a silicon photonic chip, Nature (London) **441**, 960 (2006).

[62] L. Sun, H. Wang, Y. He, Y. Zhang, G. Tang, X. He, J. Dong, and Y. Su, Broadband and fabrication tolerant power coupling and mode-order conversion using Thouless pumping mechanism, Laser Photon. Rev. **16**, 2200354 (2022).

[63] B. Zhen, C. W. Hsu, Y. Igarashi, L. Lu, I. Kaminer, A. Pick, S.-L. Chua, J. D. Joannopoulos, and M. Soljacic, Spawning rings of exceptional points out of Dirac cones, Nature (London) **525**, 354 (2015).

[64] A. Guo, G. J. Salamo, D. Duchesne, R. Morandotti, M. Volatier-Ravat, V. Aimez, G. A. Siviloglou, and D. N. Christodoulides, Observation of *PT*-symmetry breaking in complex optical potentials, Phys. Rev. Lett. **103**, 093902 (2009).

[65] A. Cerjan, S. Huang, M. Wang, K. P. Chen, Y. Chong, and M. C. Rechtsman, Experimental realization of a Weyl exceptional ring, Nat. Photon. **13**, 623 (2019).

[66] D. Kip and E. Kratzig, Anisotropic four-wave mixing in planar $LiNbO_3$ optical waveguides, Opt. Lett. **17**, 1563 (1992).

[67] D. Kip, Photorefractive waveguides in oxide crystals: Fabrication, properties, and applications, Appl. Phys. B **67**, 131 (1998).

[68] C. E. Ruter, K. G. Makris, R. El-Ganainy, D. N. Christodoulides, M. Segev, and D. Kip, Observation of parity–time symmetry in optics, Nat. Phys. **6**, 192 (2010).

[69] H. Hodaei, M.-A. Miri, M. Heinrich, D. N. Christodoulides, and M. Khajavikhan, Parity-time–symmetric microring lasers, Science **346**, 975 (2014).

[70] H. Hodaei, M.-A. Miri, A. U. Hassan, W. E. Hayenga, M. Heinrich, D. N. Christodoulides, and M. Khajavikhan, Single mode lasing in transversely multi-moded *PT*-symmetric microring resonators, Laser Photon. Rev. **10**, 494 (2016).

[71] A. Schumer, Y. G. N. Liu, J. Leshin, L. Ding, Y. Alahmadi, A. U. Hassan, H. Nasari, S. Rotter, D. N. Christodoulides, P. LiKamw, and M. Khajavikhan, Topological modes in a laser cavity through exceptional state transfer, Science **375**, 884 (2022).

[72] H. Li, R. Yao, B. Zheng, S. An, M. Haerinia, J. Ding, C.-S. Lee, H. Zhang, and W. Guo, Electrically tunable and reconfigurable topological edge state laser, Optics **3**, 107 (2022).